NANO LETTERS

2008
Vol. 8, No. 7
2027-2034

Dendrimer Templated Synthesis of One Nanometer Rh and Pt Particles Supported on Mesoporous Silica: Catalytic Activity for Ethylene and Pyrrole Hydrogenation

Wenyu Huang,[†] John N. Kuhn,[†] Chia-Kuang Tsung,[†] Yawen Zhang,[†,‡] Susan E. Habas,[†] Peidong Yang,[†] and Gabor A. Somorjai*[,†]

Department of Chemistry, University of California, Berkeley, California 94720, Chemical and Materials Sciences Divisions, Lawrence Berkeley National Laboratory, 1 Cyclotron Road, Berkeley, California 94720, and College of Chemistry and Molecular Engineering, the State Key Laboratory of Rare Earth Materials Chemistry and Applications and PKU-HKU Joint Laboratory in Rare Earth Materials and Bioinorganic Chemistry, Peking University, Beijing 100871, China

Received May 9, 2008

ABSTRACT

Monodisperse rhodium (Rh) and platinum (Pt) nanoparticles as small as ~1 nm were synthesized within a fourth generation polyaminoamide (PAMAM) dendrimer, a hyperbranched polymer, in aqueous solution and immobilized by depositing onto a high-surface-area SBA-15 mesoporous support. X-ray photoelectron spectroscopy indicated that the as-synthesized Rh and Pt nanoparticles were mostly oxidized. Catalytic activity of the SBA-15 supported Rh and Pt nanoparticles was studied with ethylene hydrogenation at 273 and 293 K in 10 torr of ethylene and 100 torr of H_2 after reduction (76 torr of H_2 mixed with 690 torr of He) at different temperatures. Catalysts were active without removing the dendrimer capping but reached their highest activity after hydrogen reduction at a moderate temperature (423 K). When treated at a higher temperature (473, 573, and 673 K) in hydrogen, catalytic activity decreased. By using the same treatment that led to maximum ethylene hydrogenation activity, catalytic activity was also evaluated for pyrrole hydrogenation.

Metal nanoparticles less than 10 nm that were monodisperse and with controlled size and shape have been synthesized by colloid techniques in recent years and characterized with a combination of techniques.[1–3] However, the synthesis of nanoparticles that are close to or smaller than 1 nm (tens of atoms) has only been attempted in a few laboratories.[4–9] For these particles, more than 90% of atoms are located on the surface[10] and the atomic coordination number of ~1 nm particles is smaller than that in larger nanoparticles (12 for an fcc lattice) which has a substantial fraction of the atoms in the bulk. At sizes smaller than ~1 nm, nanoparticles have shorter metal−metal bonds,[11,12] lower melting points,[13,14] and are easier to be oxidized than larger particles.[15,16] All of these remarkable properties for ~1 nm particles could lead to their distinctly different performance in catalytic reactions. For example, Xu et al.[17] found that the turnover frequency (TOF) of a 20 atom iridium particle was 10 times higher for toluene hydrogenation than that of a 4 atom iridium cluster. Lang et al.[8] studied the CO oxidation reaction activity of SiO_2 supported dendrimer-encapsulated Pt_{50} and Pt_{100} nanoparticles and compared it with the activity of a Pt/SiO_2 catalyst prepared using incipient wetness impregnation that yielded a wide particle size distribution. They found that the TOFs of Pt_{50}/SiO_2 were 2−3 times greater than that of Pt_{100}/SiO_2 and the incipient wetness impregnated Pt/SiO_2 catalyst. Therefore, it appears that monodisperse ~1 nm particles could yield unique catalytic properties.

A dendrimer templating strategy is very attractive for synthesis of ~1 nm nanoparticles.[18] Polyamidoamine (PAMAM) and poly(propylene imine) (PPI) are the most employed dendrimers for synthesis of metal nanoparticles. Size control of metal nanoparticles synthesized within dendrimers is realized by their well-defined functional groups and structure.[6,9,18–20] For PAMAM dendrimers, the number of internal tertiary amine functional groups, which act as ligands to

* Corresponding author. E-mail: somorjai@berkeley.edu.
† University of California and Lawrence Berkeley National Laboratory.
‡ Peking University.

10.1021/nl801325m CCC: $40.75
Published on Web 06/11/2008

Scheme 1. Synthesis of Dendrimer Encapsulated Metal Nanoparticles and the Subsequent Immobilization of the Nanoparticle on Mesoporous SBA-15 Support

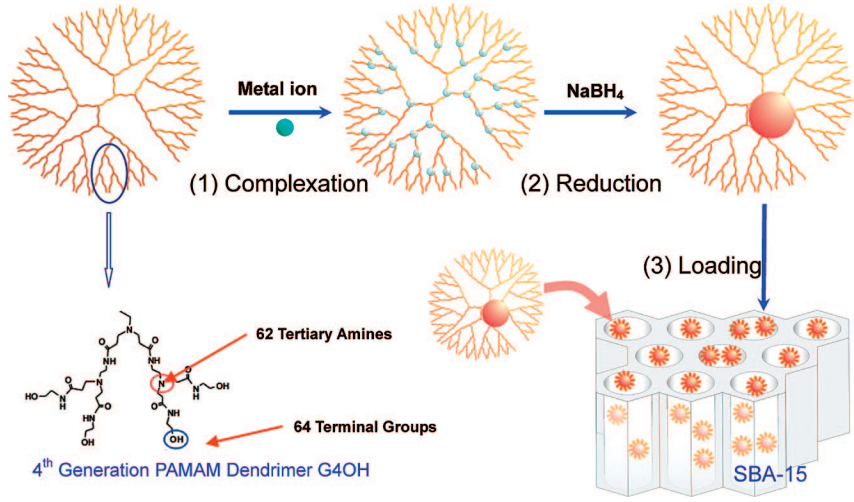

complex with metal ions, is determined by the dendrimer generation. The dendrimer provided a template for the metal ions that are deposited in the polymer (step 1 in Scheme 1). The quasispherical hyperbranched structure of the dendrimer (generation 4 and above) supplied not only internal cavities for nanoparticle growth upon reduction, but also a shell to prevent aggregation of the as-grown nanoparticles. By changing the metal ion to dendrimer concentration ratio (below maximum ion loading), nanoparticles of ~1 nm in diameter can be synthesized with narrow size distribution. Metal nanoparticles, such as Cu, Pd, and Pt, have been synthesized within the cavities of PAMAM and PPI dendrimers.[4,6,18] Bimetallic nanoparticles, such as PtPd, PdAu, PtAu, and PtCu have also been synthesized.[19–25]

Rhodium catalysts are important in catalytic reactions,[26] such as hydrogenation,[27,28] hydroformylation,[29] carbonylation,[30] and CO oxidation[31] and ~1 nm particles may lead to discovery of interesting catalytic behavior. However, the synthesis of ~1 nm Rh nanoparticles has not yet been reported to the best of our knowledge. In this communication, we report the successful synthesis of ~1 nm Rh and Pt nanoparticles in aqueous solution using dendrimer templates and the subsequent loading onto a three-dimensional (3D) support, SBA-15. X-ray photoelectron spectroscopy (XPS) and transmission electron microscopy (TEM) were used to characterize the as-synthesized nanoparticles. Compared with several commonly used methods, such as incipient wetness impregnation and coprecipitation,[32] supported nanoparticles prepared by dendrimer templating have narrower size distribution (less than 30%). After reduction in 76 torr of H_2 mixed with 690 torr of He at different temperatures, catalytic activity of the SBA-15 supported Rh and Pt nanoparticles was studied for ethylene hydrogenation (Scheme 2) and pyrrole hydrogenation (Scheme 3).

Synthesis of Rh and Pt Dendrimer Encapsulated Nanoparticles. Dendrimer encapsulated nanoparticles were synthesized following the method developed by Crooks and his co-workers[6,18,33] with minor modifications. Generation 4 dendrimers (G4OH) were purchased from Dendritech Inc. (Midland, MI) as 10.20 wt % methanol solution and used as is. A 250 μM dendrimer stock solution was prepared by adding the dendrimer methanol solution to water. The dendrimer stock solution was mixed with 15−40 mol equivalent of an aqueous solution of 0.01 M $RhCl_3$ (Rh, 38−40%) or K_2PtCl_4 (99.9+%; Sigma-Aldrich, Inc., St. Louis, MO) in a 20 mL vial. The vial was purged with Ar for 30 min and tightly sealed with a septum. The complexing process between the metal ions and the internal amine groups of the dendrimer was monitored by a UV−vis spectrometer (Agilent 8453 UV−vis ChemStation). As shown in Figure 1, absorption bands at 200, 226, and 300 nm decreased dramatically within the first 2 h of complexation, which could arise from ligand exchange reactions between chloride, water, and the internal amines within G4OH dendrimer.[34,35] After 2 h, absorption bands decreased slowly. Since the absorption spectrum only changed slightly after an 18 h exchange under static conditions for the $RhCl_3$/G4OH solution (66 h for K_2PtCl_4/G4OH solution), we choose 18 h as the complexation time for the $RhCl_3$/G4OH solution. After 18 h, 20-fold of freshly prepared 0.5 M $NaBH_4$ was injected into the vial dropwise during vigorous stirring. The $NaBH_4$ solution was kept at 0 °C before injection. The reaction solution was stirred for an additional 3 h (8 h for platinum). As shown in Figure 1, the absorption of the solution above 300 nm increased after the reduction, which indicated the formation of metal nanoparticles.[26,36] The reaction solution (10 mL) was purified by dialysis against 2 L of DI water in cellulose dialysis sacks with a molecular weight cutoff of 12 000 (Sigma-Aldrich, Inc., St. Louis, MO). Dialysis occurred over 24 h with the water being changed 4 times. The size of the nanoparticles was measured by TEM (FEI Tecnai G^2 S-Twin

Scheme 2. Ethylene Hydrogenation Reaction

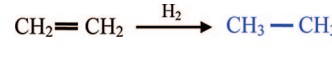

Scheme 3. Pyrrole Hydrogenation Reaction

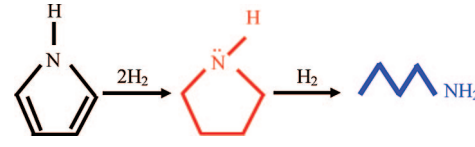

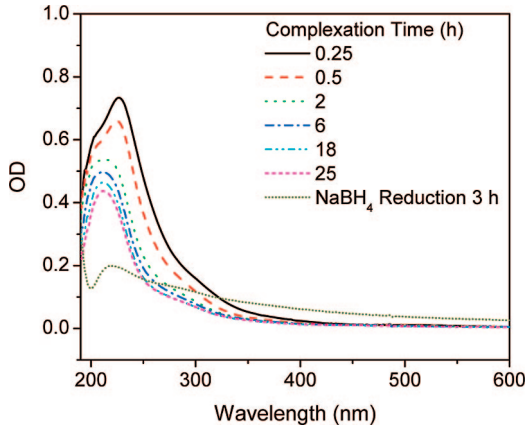

Figure 1. Time-resolved UV−vis spectra of aqueous G4OH$(Rh^{3+})_{30}$ solution and after 3 h reduction by $NaBH_4$ to yield G4OH(Rh_{30}). The concentration of G4OH is 1.6 μM. The optical path is 1.0 cm. A dendrimer solution of the same concentration is used as the background.

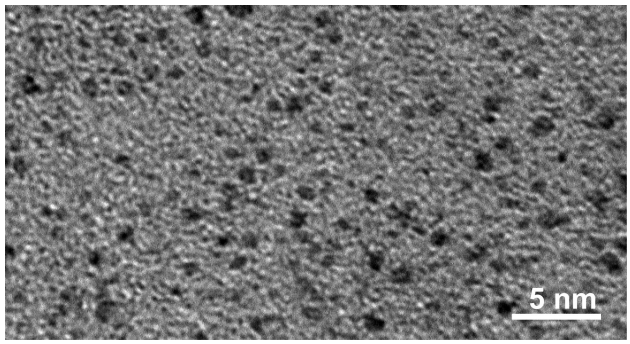

Figure 2. TEM image of G4OH(Rh_{30}) nanoparticles.

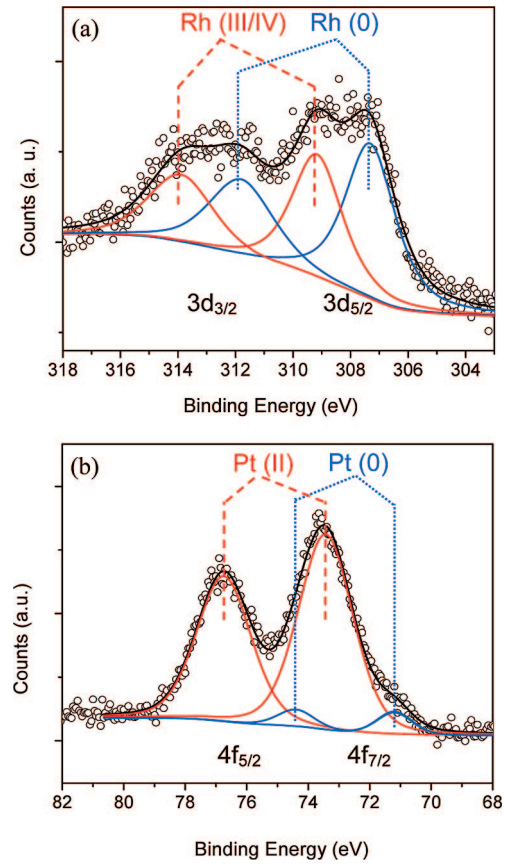

Figure 3. X-ray photoelectron spectra of dendrimer encapsulated (a) Rh_{30} and (b) Pt_{20} nanoparticles. For Rh nanoparticles, 44% of the Rh was oxidized, whereas 93% of the Pt was oxidized for the Pt nanoparticles.

electron microscope at an accelerating voltage of 200 kV). As shown by the TEM image of the G4OH(Rh_{30}) nanoparticle in Figure 2, diameters of the G4OH(Rh_{30}) nanoparticles were 1.0 ± 0.3 nm by counting more than 100 particles.

X-ray Photoelectron Spectroscopy (XPS) Study. XPS was used to characterize the dendrimer encapsulated Rh and Pt nanoparticles after deposition of the as-synthesized nanoparticle solution onto a silicon wafer. XPS experiments were performed on a Perkin-Elmer PHI 5300 XPS spectrometer with a position-sensitive detector and a hemispherical energy analyzer in an ion-pumped chamber (evacuated to 2×10^{-9} Torr). The Al K_α (BE = 1486.6 eV) X-ray source of the XPS spectrometer was operated at 300 W with 15 kV acceleration voltage.

Figure 3a shows the XPS spectrum of dendrimer encapsulated Rh_{30} nanoparticles. The Rh $3d_{5/2}$ peak was fit by two peaks with binding energies (BE) of 307.3 and 309.2 eV, corresponding to the metallic Rh (0) and oxidized Rh, respectively. Only 56% of the Rh was metallic. The remaining portion, 44% of the total Rh, was oxidized, which could be caused by air exposure during the preparation of the XPS sample and/or incomplete reduction of $RhCl_3$ during synthesis. However, the peak at 309.2 eV can not be simply assigned to Rh_2O_3 or RhO_2, whose Rh $3d_{5/2}$ peaks are around 308.3 and 308.6 eV, respectively.[37] The peak at 309.2 eV may be due to the unreduced Rh^{x+}, which formed complexes with Cl^-, H_2O, and the internal amine groups of the dendrimer. This observation also indicated that Rh complexes are strongly bound and remained within the dendrimer even after dialysis.

XPS spectra of dendrimer encapsulated Pt nanoparticles were reported,[33,38,39] but the observations were not consistent. Zhao et al.[33] observed that the Pt $4f_{7/2}$ peak appeared at 71.3 eV for dendrimer encapsulated Pt_{60} nanoparticles, which indicated complete reduction of Pt^{2+} to Pt (0). Ye et al.[38] observed that the Pt $4f_{7/2}$ peak presented at 73.0 eV for dendrimer encapsulated Pt_{30} nanoparticles. The higher binding energy of Pt_{30} nanoparticles than that of bulk Pt (0) was attributed to the effect of its small size and dendritic ligands. Ozturk et al.[39] found Pt $4f_{7/2}$ peaks located at 74.6 and 73.3 eV for dendrimer encapsulated Pt_{40} nanoparticles deposited as a thick layer and a thin layer, respectively. The authors explained the higher binding energy by the charging of the dendrimer encapsulated nanoparticle film and the incomplete reduction of Pt^{2+}. To clarify these discrepancies, we also examined the dendrimer encapsulated Pt_{20} and Pt_{40} nanoparticles using XPS.

As shown in Figure 3b, the main Pt $4f_{7/2}$ peak for the dendrimer encapsulated Pt_{20} nanoparticle was located at 73.5 eV, which is close to the observation by Ozturk et al.[39] on a thin layer of Pt_{40} nanoparticles. We think that the observed higher Pt $4f_{7/2}$ binding energy (73.5 eV) of Pt_{20} nanoparticles

($BE = 71.2$ eV for metallic Pt) was due to unreduced Pt^{2+}. The major Pt $4f_{7/2}$ peak also has a small shoulder at 71.2 eV, which was attributed to metallic Pt. From deconvolution of the Pt $4f_{7/2}$ peak, only ~7% of total Pt was metallic, which agreed with a previous EXAFS study that showed Pt remained oxidized after $NaBH_4$ exposure.[40] Similar behavior was also observed on the dendrimer encapsulated Pt_{40} nanoparticles (data not show here).

Immobilization of Dendrimer Encapsulated Rh and Pt Nanoparticles onto Mesoporous Silica SBA-15. The dendrimer encapsulated Rh and Pt nanoparticles are immobilized onto a SBA-15 silica mesoporous support before catalytic studies. The SBA-15 silica was synthesized by the method reported in the literature.[41] The SBA-15 silica support had a pore diameter of ~7 nm. The surface area and pore volume were 757 m^2 g^{-1} and 1.0 cm^3 g^{-1}, respectively. The nanoparticle solution was mixed with SBA-15, and then the slurry was sonicated for 3 h at room temperature by an ultrasonic cleaner (VWR, 75T, 120 W, 45 kHz). The nanoparticle loaded SBA-15 was separated from solution by centrifuging (Thermo Scientific IEC Centra CL2) at 4200 rpm for 6 min. After separation, the solution became colorless (dark brown color originally), which indicated the deposition of the dendrimer encapsulated Rh and Pt nanoparticles onto SBA-15. There are two possible interactions for the loading of dendrimer encapsulated nanoparticle onto SBA-15, electrostatic interaction and hydrogen bonding between dendrimer and silica.[42] First, the isoelectric point (point of zero charge) of silica material[43] is around 2, and the loading process is performed in a solution with pH of 5. At this pH, the PAMAM dendrimer is positively charged,[42] while the surface of SBA-15 silica is negatively charged. Therefore, strong electrostatic interactions existed between the dendrimer encapsulated nanoparticles and the SBA-15. Second, the PAMAM dendrimer is terminated with 64 hydroxyl groups, which could form multiple hydrogen bonds with hydroxyl groups on the surface of SBA-15 silica in water.[42]

After separation, the bottom slurry, the SBA-15 supported nanoparticle catalyst, was dried under ambient conditions for 2 days and then at 100 °C for 4 h. The dried catalyst was then finely ground. The successful loading of the dendrimer encapsulated nanoparticles onto mesoporous SBA-15 silica was confirmed by TEM and elemental analysis. The actual loadings of Rh and Pt onto SBA-15 were measured to be 0.3 and 0.6 wt. % by inductively coupled plasma (ICP) spectrometry, respectively.[44] Also, as shown in Figure 4, the nanoparticles were well-distributed over the 3D mesoporous silica support and appeared slightly larger than unsupported ones (as shown in Figure 2). However, it is very difficult to accurately measure the size of small nanoparticles on 3D supports. TEM images taken from nanoparticles loaded onto 3D supports often suffer from low contrast due to the decrease of the supporting material's electron transparency, and this behavior is magnified as particle size decreases. Nanoparticles on 3D supports are also in different focal planes during TEM imaging.[8]

Ethylene and Pyrrole Hydrogenation Reactions. Ethylene and pyrrole hydrogenation reactions were performed on the 3D mesoporous silica supported Pt and Rh catalysts at atmospheric pressure in laboratory scale flow reactors. Samples were diluted with low surface area quartz and loaded into quartz reactors. Temperature was controlled by a PID controller (Watlow 96) and a type-K thermocouple. Gas flows (all from Praxair and UHP) were regulated using calibrated mass flow controllers. Before the reaction, samples were reduced in 50 mL min^{-1} of 76 torr of H_2 with a He balance for 1 h at a desired temperature. For ethylene hydrogenation, the gases were 10 torr of ethylene, 100 torr of H_2 with a balance of He. For pyrrole hydrogenation, the feed was 4 torr of pyrrole (Sigma-Aldrich, >98%) and 400 torr of H_2 with a balance of He. The desired partial pressure of pyrrole was achieved by bubbling He through pyrrole and assuming saturation.[45] For both reactions, gas composition was analyzed with flame ionization (FID) and thermal conductivity (TCD) detectors on a HP 5890 Series II gas chromatograph (GC). No conversion was observed for either reaction when unloaded SBA-15 was tested under the same conditions. Turnover frequencies were determined by normalizing the conversion (always less than 20%) to metal surface atoms assuming 100% dispersion.

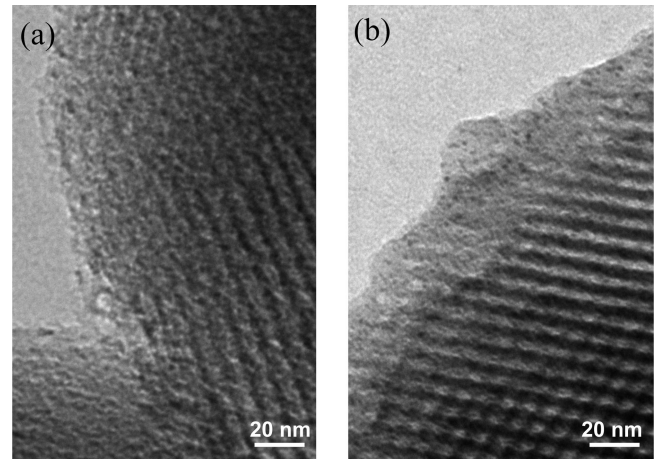

Figure 4. TEM images of dendrimer encapsulated (a) Rh_{30} and (b) Pt_{40} nanoparticle immobilized on SBA-15, denoted as Rh_{30}/SBA-15 and Pt_{40}/SBA-15, respectively.

We found that SBA-15 supported dendrimer capped Rh_{30} and Pt_{20} nanoparticles have activity for ethylene hydrogenation without any pretreatment (Figure 5). Moreover, we evaluated the effect of reduction (76 torr of H_2 with a He balance) at different temperatures upon ethylene hydrogenation activity for the SBA-15 supported Rh_{30} and Pt_{20} catalysts. As shown in Figure 5, the highest activity occurred for both the Rh_{30}/SBA-15 and the Pt_{20}/SBA-15 catalysts after reducing the samples at 423 K for 1 h. After this low temperature reduction, the TOF of Rh_{30}/SBA-15 increased from 0.60 to 0.83 s^{-1}, and the TOF of Pt_{20}/SBA-15 increased from 0.5 to 3.7 s^{-1} when the ethylene hydrogenation reaction was carried at 293 K. This mild pretreatment condition did not cause any observable sintering of dendrimer encapsulated Rh and Pt nanoparticles by TEM, which is crucial for studying catalysis over ~1 nm particles. The activity increase for the Rh_{30}/SBA-15 and Pt_{20}/SBA-15 catalysts after the low temperature treatment in 76 torr of H_2 with a He balance was

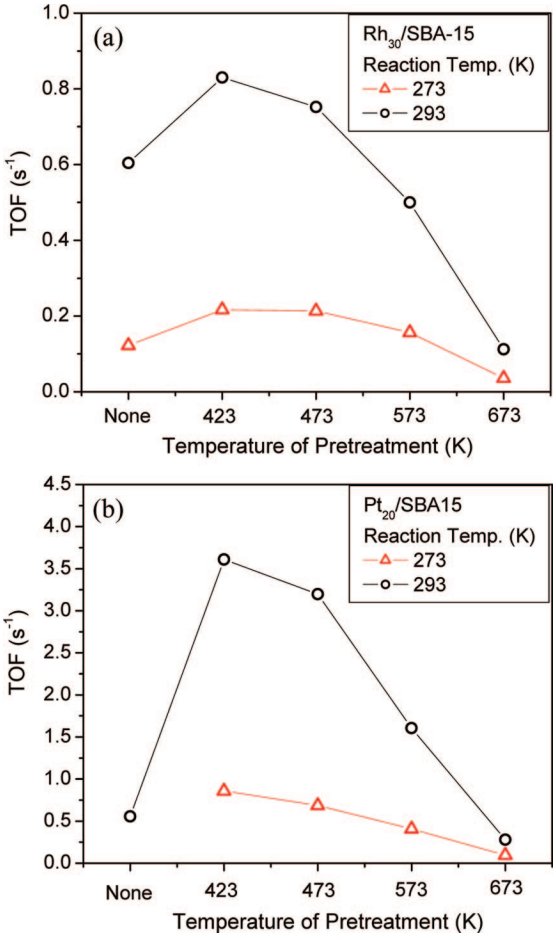

Figure 5. Initial ethylene hydrogenation activity over (a) Rh_{30}/SBA-15 and (b) Pt_{20}/SBA-15 after reducing in 76 torr of H_2 balanced with He at different temperature. Reaction mixture was 10 torr C_2H_4 and 100 torr H_2.

due to the reduction of oxidized Rh and Pt to Rh (0) and Pt (0), which are both more active for hydrogenation reactions than the respective oxidized species. As discussed before, XPS showed that the as-synthesized Rh_{30} and Pt_{20} nanoparticles contained a large portion of oxidized species so reduction during exposure to 76 torr of H_2 with a balance of He at 423 K for 1 h is plausible. Partial decomposition of dendrimer capping by reduction[46] at 423 K could also contribute to the increase of reaction activity. After reduction at 473 K for 1 h in 76 torr of H_2 with a balance of He, TOFs for Rh_{30}/SBA-15 and Pt_{20}/SBA-15 decreased slightly. When the reduction temperature was further raised to 573 K, TOFs for Rh_{30}/SBA-15 and Pt_{20}/SBA-15 again decreased. After reduction at 673 K, severe deactivation of Rh_{30}/SBA-15 and Pt_{20}/SBA-15 catalysts was observed. Since TOFs were calculated assuming 100% dispersion, decreased activity after high temperature treatments was most likely due to sintering of supported Rh_{30} and Pt_{20} nanoparticles, which resulted in a decrease in the number of active sites. A TEM image (Figure 6) of the Rh_{30}/SBA-15 catalyst after thermal treatment at 673 K for 1 h showed that severe sintering of the Rh_{30} nanoparticle occurred. However, other reasons for the deactivation, such as coke formation from dendrimer decomposition, cannot be excluded.

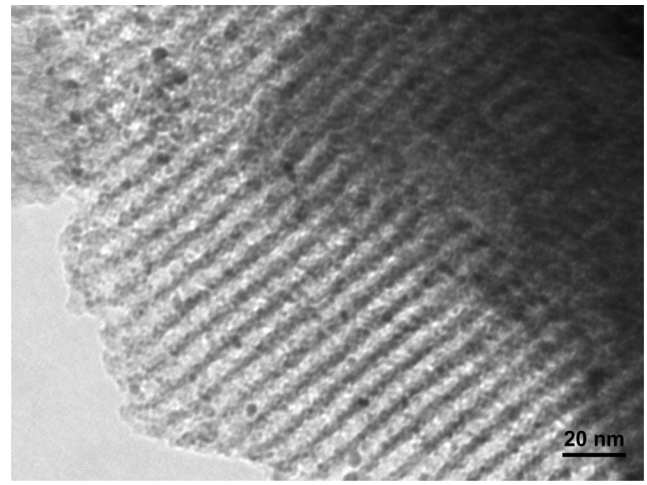

Figure 6. TEM image of the dendrimer encapsulated Rh_{30} nanoparticle, after heating in 76 torr of H_2 with He balance at 673 K for 1 h. Many nanoparticles larger than 2 nm are observed because of the sintering of small Rh_{30} nanoparticles.

In Table 1, initial ethylene hydrogenation activities for SBA-15 supported dendrimer Rh and Pt catalysts are compared to PVP capped nanoparticles and Pt(111) and Rh(111) single crystals. Ethylene hydrogenation activity was measured over PVP capped Rh nanoparticles at 350 K, but activation energies were not reported.[26] By converting our data over Rh_{15}/SBA-15 and Rh_{30}/SBA-15 catalysts to 350 K, TOFs were $\sim$32 s^{-1}, which was higher than that of the PVP capped Rh nanoparticles. TOFs for the Rh_{15}/SBA-15 and Rh_{30}/SBA-15 catalysts were lower compared with the Rh(111) single crystal at 298 K. For the dendrimer encapsulated Pt catalysts, TOFs were lower than that of the Pt(111) single crystal but comparable to PVP capped Pt nanoparticles. The lower TOFs of the dendrimer encapsulated nanoparticles compared with single crystals were likely caused by the dendrimer capping, which could block a portion of the active sites. Other factors, such as support interactions or size induced property changes (i.e., electron deficiency) for $\sim$1 nm particles, are also likely involved. Activation energies (Table 1) for the Rh_{15}/SBA-15 and Rh_{30}/SBA-15 catalysts were only slightly higher than that of the Rh(111) single crystal. For the Pt_{20}/SBA-15 and Pt_{40}/SBA-15 catalysts, activation energies followed similar trends.

Catalytic activity over these dendrimer encapsulated nanoparticles was also exhibited by performing pyrrole hydrogenation (Figure 7). Both Rh catalysts displayed similar activities and 100% selectivity to pyrrolidine. Moreover, Rh catalysts displayed higher activity than the Pt catalysts. However, over the Pt catalysts, the reaction was able to proceed beyond just the first step as *n*-butylamine became a prominent product (Rh catalysts produced only pyrrolidine at these temperatures, data not shown). Butane was also observed as a minor product over Pt (not shown). These results were in agreement with single crystal kinetic data, which showed TOFs of $\sim$0.05 s^{-1} between 298 and 413 K over both Pt(111) and Rh(111) surfaces and more C−N bond scission over the Pt(111) surface than the Rh(111) surface.[47] As supported by several pieces of evidence, these results

Table 1. Ethylene Hydrogenation Rates and Activation Energy on SBA-15 Supported Rh and Pt Nanoparticles

catalyst	theoretical number of metal atoms per particle[a]	E_a (kcal/mol)	initial TOF at 298 K (s^{-1})[b,c]
Rh_{15}/SBA-15	15	11.4	1.0
Rh_{30}/SBA-15	30	12.3	1.0
Rh NPs[26]	7−33 k	∼	0.5[d]
Rh (111)[52]	∼	8.0	4.2
Pt_{20}/SBA-15	20	12.2	4.3
Pt_{40}/SBA-15	40	11.5	3.3
Pt NPs[53]	0.2−10 k	10	3.5
Pt (111)[54]	∼	10.8	6.1

[a] For Rh and Pt NPs, the number of metal atoms per nanoparticle is estimated by assuming a spherical shape. [b] Initial rates corrected to 10 torr C_2H_4, 100 torr H_2, and 298 K using corresponding activation energies and assuming zero order and first order dependence for ethylene and H_2, respectively. The dendrimer encapsulated Rh and Pt nanoparticle catalysts were pretreated with 76 torr of H_2 and 690 torr of He at 423 K for 1 h. [c] For dendrimer encapsulated Rh and Pt nanoparticles, initial TOF was calculated based on 100% metal dispersion. [d] Reaction conditions were 20 torr C_2H_4, 100 torr H_2, and 350 K.

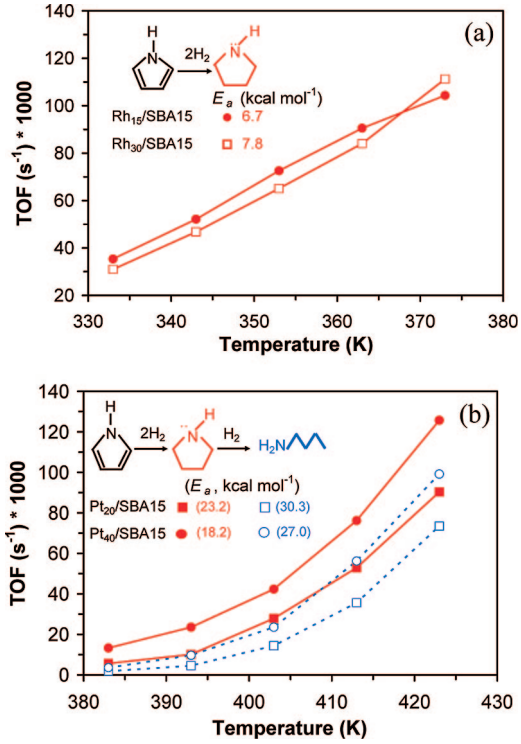

Figure 7. Reaction results for pyrrole hydrogenation over (a) Rh_{15}/SBA-15 and Rh_{30}/SBA-15 and (b) Pt_{20}/SBA-15 and Pt_{40}/SBA-15 catalysts. Catalysts were reduced at 423 K in 76 torr of H_2 mixed with He in the ratio of 1:10 for 1 h prior to the reaction. Reaction conditions were 4 torr pyrrole and 400 torr H_2.

are caused by *n*-butylamine poisoning of the catalyst surfaces. First, sum-frequency generation spectra over Pt(111) and Rh(111) surfaces demonstrated no N−H bands at 363 K, which suggested strong Pt−N (no H binding to N) interactions.[47] Second, butane formation was reported to occur more rapidly over Pt supported catalysts when pyrrolidine was used as the reactant rather than *n*-butylamine.[48] Additionally, we also found that the Pt_{20}/SBA-15 and Pt_{40}/SBA-15 catalysts were very stable during pyrrole and ethylene hydrogenation. On the other hand, the Rh_{15}/SBA-15 and Rh_{30}/SBA-15 catalysts lost ∼30% of their activity after 10 h of ethylene hydrogenation, and similar results were observed during pyrrole hydrogenation over 3 h. Complete analyses of these results, including comparison to larger nanoparticles (2 to 10 nm) prepared by other synthetic procedures, demonstrated that pyrrole hydrogenation is structure sensitive and will be performed in a future publication.

Discussion of Catalytic Activity. It was reported previously that the dendrimer encapsulated Pt nanoparticles had no activity before removing the dendrimer capping.[8,9] It was proposed that dendrimer collapsed onto the nanoparticle surface upon drying and blocked all active sites.[8,9,49] Even for small molecules like CO, FTIR studies showed that it can not adsorb onto dendrimer encapsulated Pt nanoparticle surfaces when the dendrimer encapsulated nanoparticle was supported and dried on silica and γ-Al_2O_3 supports.[9,49] High temperature thermal treatments (>300 °C) in O_2 and H_2 were needed to activate the dendrimer encapsulated nanoparticle.[40,42,50] However, high temperature treatments usually induce aggregation for small nanoparticles. For example, Sun et al.[42] found the height of a dendrimer encapsulated Pd_{40} nanoparticle increased from 0.8 to 2.4 nm on a plane mica surface after flowing O_2 at 903 K for 10 min. The decrease in the density of Pd_{40} nanoparticles suggested that the nanoparticles diffuse on the mica surface during the thermal treatment and agglomerate.[42] When dendrimer encapsulated Pt_{40} nanoparticles were deposited on γ-Al_2O_3, an EXAFS study[40] showed that the nanoparticles increased from ∼1 nm to above 4 nm after a treatment at 673 K. Even when the dendrimer encapsulated Au or Pd nanoparticles were embedded within a titania support, Scott et al.[51] found that the nanoparticle size increased from 2 to 2.7 nm after calcination at 773 K. The diameter of the nanoparticles further increased to 4.4 nm when the calcination temperature was 823 K. Similar behavior was also observed for titania-supported PdAu bimetallic nanoparticles.[24]

To study catalysis over ∼1 nm particles, their aggregation induced by high temperature treatments should be avoided. We used an ordered mesoporous silica support, which might reduce the dendrimer collapse on the nanoparticle surface before any thermal pretreatment and keep a larger potion of the nanoparticle surface available for catalysis compared with amorphous silica and γ-Al_2O_3 supported nanoparticles.[8,9,46] The mesoporous SBA-15 used in this study has closely packed parallel channels with a diameter of 7 nm, which is just slightly larger than the diameter of a generation 4 PAMAM dendrimer. When the dendrimer encapsulated nanoparticles are loaded into the channels of SBA-15, the internal surface of the channel could provide a 3D support

for the dendrimer framework by strong electrostatic interactions and hydrogen bonding between the terminal hydroxyl groups of G4OH dendrimers and the internal surfaces of SBA-15. These could render the surface of dendrimer encapsulated metal nanoparticles accessible to reactants during catalytic reactions.

Conclusion. Synthesis of ~1 nm monodisperse Pt and Rh nanoparticles was demonstrated using a dendrimer templating approach. XPS indicated that the as-synthesized Rh and Pt nanoparticles were mostly oxidized. Dendrimer encapsulated nanoparticles were immobilized onto a high-surface-area SBA-15 mesoporous support by electrostatic and hydrogen bonding interactions between the dendrimers and the silica support. Catalysts were active for ethylene hydrogenation without any pretreatment, which could be due to the 3D support provided by SBA-15. The 3D support may prevent dendrimer collapsing on the nanoparticle surface and blocking of their active sites. After a mild reduction (423 K) in 76 torr of H_2 with He balance, catalytic activity was maximized for ethylene hydrogenation because of the reduction of the oxidized Rh and Pt in the as-synthesized nanoparticles. Existence of catalytic activity and preservation of the small particle size after low temperature treatments represents a significant advance for further reaction studies over these small nanoparticles. Reduction at higher temperatures (473, 573, and 673 K) led to decreased activity and was believed to be caused by sintering. Catalytic activity was further demonstrated over the dendrimer encapsulated nanoparticles for the pyrrole hydrogenation reaction.

Acknowledgment. This work was supported by the Director, Office of Science, Office of Basic Energy Sciences, Division of Chemical Sciences, Geological and Biosciences of the U.S. Department of Energy under Contract No. DE-AC03-76SF00098. This work was also supported by the Director, Office of Science, Office of Basic Energy Sciences, Division of Materials Sciences and Engineering of the U.S. Department of Energy under Contract No. DE-AC02-05CH11231. We thank the Molecular Foundry of the Lawrence Berkeley National Laboratory for using their facilities. We thank Professor A. Paul Alivisatos for use of the TEM. Y.W.Z. appreciates the financial aid of Huaxin Distinguished Scholar Award from Peking University Education Foundation of China.

References

(1) El-Sayed, I. H.; Huang, X. H.; El-Sayed, M. A. *Nano Lett.* **2005**, *5*, 829–834.
(2) Wang, Z. L.; Kang, Z. C. *Functional and Smart Materials: Structural Evolution and Structure Analysis; 1st edition ed.*; Plenum Press: New York, 1998.
(3) Ferrando, R.; Jellinek, J.; Johnston, R. L. *Chem. Rev.* **2008**, *108*, 845–910.
(4) Balogh, L.; Tomalia, D. A. *J. Am. Chem. Soc.* **1998**, *120*, 7355–7356.
(5) Esumi, K.; Suzuki, A.; Aihara, N.; Usui, K.; Torigoe, K. *Langmuir* **1998**, *14*, 3157–3159.
(6) Crooks, R. M.; Zhao, M. Q.; Sun, L.; Chechik, V.; Yeung, L. K. *Acc. Chem. Res.* **2001**, *34*, 181–190.
(7) Floriano, P. N.; Noble, C. O.; Schoonmaker, J. M.; Poliakoff, E. D.; McCarley, R. L. *J. Am. Chem. Soc.* **2001**, *123*, 10545–10553.
(8) Lang, H. F.; May, R. A.; Iversen, B. L.; Chandler, B. D. *J. Am. Chem. Soc.* **2003**, *125*, 14832–14836.
(9) Deutsch, D. S.; Lafaye, G.; Liu, D. X.; Chandler, B.; Williams, C. T.; Amiridis, M. D. *Catal. Lett.* **2004**, *97*, 139–143.
(10) Higatsberger, M. J. In *Advances in Electronics and Electron Physics*; Marton, C., Ed.; Academic Press: New York, 1981; Vol. 56.
(11) Apai, G.; Hamilton, J. F.; Stohr, J.; Thompson, A. *Phys. Rev. Lett.* **1979**, *43*, 165.
(12) Balerna, A.; Bernieri, E.; Picozzi, P.; Reale, A.; Santucci, S.; Burattini, E.; Mobilio, S. *Phys. Rev. B* **1985**, *31*, 5058.
(13) Wang, Z. L.; Petroski, J. M.; Green, T. C.; El-Sayed, M. A. *J. Phys. Chem. B* **1998**, *102*, 6145–6151.
(14) Huang, W. Y.; Qian, W.; El-Sayed, M. A. *J. Phys. Chem. B* **2005**, *109*, 18881–18888.
(15) Cai, W. P.; Zhong, H. C.; Zhang, L. D. *J. Appl. Phys.* **1998**, *83*, 1705–1710.
(16) Brandes, E. A., Ed. *Smithells Metals Reference Book, 6th ed.*; Butterworths: London, 1983.
(17) Xu, Z.; Xiao, F. S.; Purnell, S. K.; Alexeev, O.; Kawi, S.; Deutsch, S. E.; Gates, B. C. *Nature* **1994**, *372*, 346–348.
(18) Scott, R. W. J.; Wilson, O. M.; Crooks, R. M. *J. Phys. Chem. B* **2005**, *109*, 692–704.
(19) Lang, H.; Maldonado, S.; Stevenson, K. J.; Chandler, B. D. *J. Am. Chem. Soc.* **2004**, *126*, 12949–12956.
(20) Hoover, N. N.; Auten, B. J.; Chandler, B. D. *J. Phys. Chem. B* **2006**, *110*, 8606–8612.
(21) Scott, R. W. J.; Datye, A. K.; Crooks, R. M. *J. Am. Chem. Soc.* **2003**, *125*, 3708–3709.
(22) Chung, Y. M.; Rhee, H. K. *Catal. Lett.* **2003**, *85*, 159–164.
(23) Knecht, M. R.; Weir, M. G.; Frenkel, A. I.; Crooks, R. M. *Chem. Mater.* **2008**, *20*, 1019–1028.
(24) Scott, R. W. J.; Sivadinarayana, C.; Wilson, O. M.; Yan, Z.; Goodman, D. W.; Crooks, R. M. *J. Am. Chem. Soc.* **2005**, *127*, 1380–1381.
(25) Scott, R. W. J.; Wilson, O. M.; Oh, S. K.; Kenik, E. A.; Crooks, R. M. *J. Am. Chem. Soc.* **2004**, *126*, 15583–15591.
(26) Zhang, Y.; Grass, M. E.; Habas, S. E.; Tao, F.; Zhang, T.; Yang, P.; Somorjai, G. A. *J. Phys. Chem. C* **2007**, *111*, 12243–12253.
(27) Pellegatta, J. L.; Blandy, C.; Colliere, V.; Choukroun, R.; Chaudret, B.; Cheng, P.; Philippot, K. *J. Mol. Catal. A: Chem.* **2002**, *178*, 55–61.
(28) Park, K. H.; Jang, K.; Kim, H. J.; Son, S. U. *Angew. Chem., Int. Ed.* **2007**, *46*, 1152–1155.
(29) Yoon, T. J.; Kim, J. I.; Lee, J. K. *Inorg. Chim. Acta* **2003**, *345*, 228–234.
(30) Halttunen, M. E.; Niemela, M. K.; Krause, A. O. I.; Vaara, T.; Vuori, A. I. *Appl. Catal., A* **2001**, *205*, 37–49.
(31) Park, J. Y.; Zhang, Y.; Grass, M.; Zhang, T.; Somorjai, G. A. *Nano Lett.* **2008**, *8*, 673–677.
(32) Ertl, G.; Knö zinger, H.; Weitkamp, J. *Handbook of Heterogeneous Catalysis;* Wiley/VCH: New York, 1997.
(33) Zhao, M. Q.; Crooks, R. M. *Adv. Mater.* **1999**, *11*, 217–220.
(34) Benguerel, E.; Demopoulos, G. P.; Harris, G. B. *Hydrometallurgy* **1996**, *40*, 135–152.
(35) Kuno, K.; Ito, J. *Nippon Kagaku Kaishi* **1995**, 432–439.
(36) Kreibig, U.; Vollmer, M. *Optical properties of metal clusters*; Berlin: New York, 1995.
(37) Abe, Y.; Kato, K.; Kawamura, M.; Sasaki, K. *Surf. Sci. Spectra* **2001**, *8*, 117.
(38) Ye, H. C.; Scott, R. W. J.; Crooks, R. M. *Langmuir* **2004**, *20*, 2915–2920.
(39) Ozturk, O.; Black, T. J.; Perrine, K.; Pizzolato, K.; Williams, C. T.; Parsons, F. W.; Ratliff, J. S.; Gao, J.; Murphy, C. J.; Xie, H.; Ploehn, H. J.; Chen, D. A. *Langmuir* **2005**, *21*, 3998–4006.
(40) Alexeev, O. S.; Siani, A.; Lafaye, G.; Williams, C. T.; Ploehn, H. J.; Amiridis, M. D. *J. Phys. Chem. B* **2006**, *110*, 24903–24914.
(41) Zhao, D.; Huo, Q.; Feng, J.; Chmelka, B. F.; Stucky, G. D. *J. Am. Chem. Soc.* **1998**, *120*, 6024–6036.
(42) Sun, L.; Crooks, R. M. *Langmuir* **2002**, *18*, 8231–8236.
(43) Iler, R. K. *The Chemistry of Silica*; John Wiley & Sons: New York, 1979.
(44) The ICP analysis of Pt is performed by Galbraith Laboratories, Inc. (Knoxville, TN). For Rh, the analysis is performed by Mikroanalytisches Labor Pascher (Remagen-Bandorf, Germany). For the Rh catalysts, similar metal loadings were also determined by electron probe microanalysis (EPMA; Earth and Planetary Science, University of California Berkeley, Berkeley, CA).
(45) Das, A.; Frenkel, M.; Gadalla, N. A. M.; Kudchadker, S.; Marsh, K. N.; Rodgers, A. S.; Wilhoit, R. C. *J. Phys. Chem. Ref. Data* **1993**, *22*, 659.

(46) Deutsch, D. S.; Siani, A.; Fanson, P. T.; Hirata, H.; Matsumoto, S.; Williams, C. T.; Amiridis, M. D. *J. Phys. Chem. C* **2007**, *111*, 4246–4255.
(47) Kliewer, C. J.; Bieri, M.; SomorjaiG. A. *J. Phys. Chem. C*, accepted
(48) Triyono, n/a.; Kramer, R. *Appl. Catal., A* **1993**, *100*, 145–155.
(49) Liu, D.; Gao, J.; Murphy, C. J.; Williams, C. T. *J. Phys. Chem. B* **2004**, *108*, 12911–12916.
(50) Lafaye, G.; Siani, A.; Marecot, P.; Amiridis, M. D.; Williams, C. T. *J. Phys. Chem. B* **2006**, *110*, 7725–7731.
(51) Scott, R. W. J.; Wilson, O. M.; Crooks, R. M. *Chem. Mater.* **2004**, *16*, 5682–5688.
(52) Bent, B. E. *Bonding and Reactivity of Unsaturated Hydrocarbons on Transition Metal Surfaces: Spectroscopic and Kinetic Studies of Platinum and Rhodium Single Crystal Surfaces. Ph.D. Thesis*, University of California, Berkeley, CA, 1986.
(53) Song, H.; Rioux, R. M.; Hoefelmeyer, J. D.; Komor, R.; Niesz, K.; Grass, M.; Yang, P.; Somorjai, G. A. *J. Am. Chem. Soc.* **2006**, *128*, 3027–3037.
(54) Zaera, F.; Somorjai, G. A. *J. Am. Chem. Soc.* **1984**, *106*, 2288–2293.

NL801325M